International Journal of Lightweight Materials and Manufacture 5 (2022) 29–43

Contents lists available at ScienceDirect

International Journal of Lightweight Materials and Manufacture

journal homepage: www.keaipublishing.com/en/journals/international-journal-of-lightweight-materials-and-manufacture

Impact damage resistance of novel adhesively bonded natural fibre composite – Steel hybrid laminates

Karthik Ram Ramakrishnan [a, b, *], Mikko Kanerva [a], Essi Sarlin [a], Mikko Hokka [a]

[a] Engineering Materials Science, Faculty of Engineering and Natural Sciences, Tampere University, Tampere, 33014, Finland
[b] Bristol Composites Institute, University of Bristol, Bristol, BS8 1TR, United Kingdom

ARTICLE INFO

Article history:
Received 16 August 2021
Received in revised form
28 September 2021
Accepted 3 October 2021
Available online 13 October 2021

Keywords:
Natural fibre composites
Impact resistance
Hybrid composites
DIC
Finite element analysis

ABSTRACT

Synthetic fibre reinforcements are increasingly replaced with plant fibres but an improvement in the mechanical performance of biocomposites is required. Flax composite exhibits fibre failure and perforation even at low impact energies. This paper investigates the viability of improving the impact resistance of flax-epoxy biocomposite by hybridisation with a thin metal layer. High-speed cameras and optical microscopy were used to measure the dissipated energy and to identify the different damage modes. The impact response of hybrid biocomposites was compared to a reference GFRP composite and monolithic biocomposites and it was shown that the deformation and damage is significantly reduced in the hybrid configuration. Additionally, a numerical model was developed in Abaqus/Explicit and validated in terms of the displacement history and damage modes. The study reveals the effect of various material configurations and thicknesses on impact damage resistance and proves that the penetration resistance of biocomposites is improved by hybrid construction.

1. Introduction

Biocomposites reinforced with lignocellulosic natural fibres are an emerging class of lightweight materials with high specific properties and positive environmental profile, and are considered as potential replacement to the synthetic composites currently used in structural applications [1]. In particular, specific mechanical properties of flax fibre composites are comparable to those of GFRP [2,3]. Bourmaud et al. [4] concluded from a detailed study on the design considerations of high performance plant fibre composites that flax fibre performs exceptionally well in the strength selection criteria due to the large length of the elementary fibres and high fibre division of the unidirectional flax that promotes good stress-transfer between fibre and matrix. However, Pil et al. [3] indicated that the adoption of natural fibres in structural applications was hindered by the inadequate data on the impact damage resistance of these composites. It has been reported that impact damage is one of the most critical types of failure in composite structures. Impact loading can occur during the service life by dropped tools, falling cargo, maintenance damage (low velocity) or high velocity events such as bird strike and ballistic impact. Composite laminates are more susceptible to impact damage as they are brittle and absorb impact energy primarily through damage mechanisms such as matrix cracking, delamination, fibre breakage and failure. The internal damage in the composite can rapidly diminish the structural integrity and cause catastrophic failure. Several researchers [5–12] have evaluated the impact behaviour of plant fibre reinforced composites with thermoset and thermoplastic matrices using a drop tower or pendulum impactors. For instance, Liang et al. [8] studied the low velocity impact behaviour of quasi-isotropic laminates of flax/epoxy and used force – deflection curves, rear face crack length, energy absorbed, and microstructural observations to study the evolution of damage from delaminations to large macro cracks. Bensadoun et al. [9] investigated the effect of matrix material and fibre architecture on the impact behaviour of flax fibre composites and found that the matrix ductility was a critical factor in both the damage resistance and damage tolerance. Although the low velocity impact behaviour of flax composites has been studied by many researchers, there is limited comparison of the impact response of natural fibre

* Corresponding author. Engineering Materials Science, Faculty of Engineering and Natural Sciences, Tampere University, Tampere, 33014, Finland.
E-mail address: karthik.ramakrishnan@bristol.ac.uk (K.R. Ramakrishnan).
Peer review under responsibility of Editorial Board of International Journal of Lightweight Materials and Manufacture.

https://doi.org/10.1016/j.ijlmm.2021.10.001

composites to that of glass fibre composites. Barouni and Dhakal [10] compared the impact response of flax and glass fibre (GFRP) composites at two different impact energies (25 J and 50 J) and observed that while the flax specimens absorbed more energy, they exhibited much greater damage compared to the glass fibre composite. Patel et al. [13] compared natural fibre composites and GFRP and found the impact performance of biocomposites were inferior even after surface treatments and additional fillers.

Hybridisation has drawn the attention of many researchers as a way to enhance the mechanical properties of polymer composites with natural fibre reinforcements. Lightweight hybrid materials can be produced by combining distinct materials to achieve a synergistic effect through proper material design. The performance of the hybrid composite is a weighted sum of the individual components, where the advantages of one material could complement what is lacking in the other. The hybrid construction enables to achieve desirable outcomes such as functional properties (vibration/acoustic damping, anti-corrosion, and impact resistance), reduced energy consumption, and improvements in structural performance and cost efficiency not achievable by individual constituent materials. For instance, Selver et al. [14] investigated the impact and post-impact behaviour of composites reinforced with glass, flax, jute fabrics and their hybrid combinations (glass/jute and glass/flax) and showed that the hybrid composites have better damage tolerance than the natural fibre and glass composites. Fibre Metal Laminates (FML) are a type of hybrid materials that merge the advantages of plastic behaviour and durability offered by metallic materials to the superior fatigue properties of FRP composites. One of the successful examples of FML that has been commonly embraced in the aircraft industry is GLARE, which is a hybrid of glass fibre-reinforced epoxy and aluminium. Reyes and Cantwell [15] demonstrated that FMLs absorbed substantial energy by means of plastic deformation of the metal layer. The failure process of FMLs is a mixture of debonding in the metal-composite interlayer, and matrix cracking, delamination and fibre fracture failure modes in composite [16]. Sarlin et al. [17,18] developed steel/composite hybrid structures with rubber as an adhesive layer and found that the damage area in impact tests was significantly reduced. The use of thin steel layers and elastomers to improve the delamination resistance and residual strength of glass and carbon FRPs have been explored [19]. The crashworthiness of composite-intensive FRP-metal hybrid materials have been investigated by a combination of experimental and numerical techniques and it was reported that the hybrid material provided stable and robust energy absorption, outperforming conventional materials [20]. It has also been shown that using a validated Finite Element (FE) model will allow to study the effect of parameters such as impact velocity, layer thicknesses as well as incident angle on the impact behaviour of these hybrid composites [21]. Although there is considerable literature showing the success of FRP-metal hybrids with GFRP and CFRP, hybrid materials with natural fibre composite layers has received significantly far less attention [22]. A study of FMLs with different natural fibres and aluminium showed improvement in mechanical properties for the hybrid materials [23]. The indentation behaviour of Kenaf-Aluminium FMLs showed a several-fold increase in the energy absorbed in comparison to composites without metal layers [24]. Wambua et al. [25] confirmed that the ballistic limit of steel-flax hybrid material was significantly higher compared to flax composite and also reported that the energy dissipation of the hybrid material was even superior to mild steel. Conversely, the performance of the flax-FML composite was found to be inferior to that of the glass-FML hybrid composite [26]. Santulli et al. [27] concluded that obtaining damage tolerance of natural fibre metal laminates that is comparable to GLARE was still a scientifically challenging task.

It is clear from the presented literature that the impact damage resistance of natural fibre reinforced composites is lower than that of traditional GFRP composites and that the hybridisation provides a potential path to enhance the mechanical properties of biocomposites. This paper deals with the development of a novel hybrid laminate, in which a thin steel layer is adhesively bonded to a flax fibre-epoxy composite and the assessment of the impact damage resistance using a combination of experiments and simulations. The viability of adhesively bonded joint between the steel layer and the natural fibre composite was verified in our earlier publication using single lap joint testing [28]. The experimental study of the impact damage resistance of this hybrid laminate was performed using a High Velocity Particle Impactor (HVPI), while a finite element model is implemented in Abaqus Explicit software to simulate the dynamic behaviour of the hybrid laminate.

2. Materials and methods

2.1. Materials

The natural fibre reinforcement used for the biocomposite was Biotex Flax developed by Composites Evolution. The [0/90] woven fabric with areal density of 400 g/m^2 was made of twistless flax fibres in a balanced 2x2-twill architecture. A reference glass fibre material of [0/90] plain woven ECR-glass fabric with areal density of 400 g/m^2 supplied by Ahlstrom-Munksjö was also chosen for the study. Araldite LY5052 epoxy resin and Araldur 5052 polyamine hardener mixed in the ratio of 100:38 by weight according to supplier recommendations was used as the matrix. The metal layer chosen for the hybrid laminate was a thin sheet of ferritic stainless steel (Type 1.4509) supplied by Outokumpu Stainless Oyj. The thickness of the steel layer was 0.48 ± 0.01 mm.

2.2. Manufacturing of hybrid laminate

The fabrication of the hybrid composite followed a two-step procedure. Initially the composites were manufactured using a hand-layup procedure and cured in a hotpress compression moulding system. A wet layup and compression moulding process was used for the manufacturing of GFRP composite with eight plies and flax composite with four plies. More details on the manufacturing procedure is presented in Refs. [28,29].The fibre volume fraction (V_f) was estimated based on the mass of the dry fabric and the mass of the cured composite. The V_f for the glass-epoxy and flax-epoxy composites were 65.9% and 40.5%, respectively. The average thickness of the cured composites were 2.64 ± 0.03 mm and 3.78 ± 0.1 mm for the composites with glass and flax fibre reinforcements, respectively. The flax composite and GFRP were considered comparable even though fibre volume fraction and thickness were different, as they had equivalent mass of approximately 25 g for square plates of dimension 80 × 80 mm cut from the manufactured composites.

In the second step of the manufacturing the hybrid laminates, the manufactured composites were adhesively bonded to the thin ferritic stainless steel sheet supplied by Outokumpu Stainless Oyj. The adhesion between stainless steel and composite layer is critical and improved solutions for the bonding of biocomposite hybrids are needed [30]. 3 M™ Scotch-Weld™ DP460, a commercial epoxy adhesive which has good peel, shear, and impact properties was used for bonding the steel and composite layers.

2.3. Experimental setup for impact testing

The experimental impact tests were conducted using a High Velocity Particle Impactor (HVPI), an in-house developed device,

shown in Fig. 1. The HVPI uses compressed air to accelerate a 2.98 g steel ball (9 mm diameter) along a smooth barrel towards the target plate. The target was clamped in a fixture housed in a transparent polycarbonate case to act as a protective barrier for the projectile and debris. The velocity of the projectile exiting the barrel was measured using a commercial ballistic chronograph and can be varied by changing the pressure. In our study, pressures of 0.2 MPa and 0.6 MPa were used corresponding to initial velocities of 45 m/s and 73 m/s respectively. The initial energies of the impacting projectiles were approximately 3 J and 8 J. A high speed camera (Memrecam) was also placed perpendicular to the path of the projectile to record images at a frame rate of 10,000 fps and resolution of 448 × 368 pixels. It is possible to measure the initial impact velocity and rebound velocity from the high speed images.

Additionally, two Photron SA-X2 high-speed cameras were positioned behind the target to monitor the rear surface of the target during the impact, and the recorded images were used for stereo digital image correlation (DIC). The images were acquired at a frame rate of 120 k fps and a resolution of 256 × 256 pixels. The start of the image acquisition was triggered by a signal from the pressure control valve. LaVision DaVis was the software used for recording and image processing of high speed camera images. Stereo-DIC analysis was conducted on the images of the rear surface of the target obtained from the Photron cameras. DIC is based on the principle of tracking the movement of small subsets in consecutive digital images of the specimen surface, which has a random pattern of high contrast speckles. A comparison of subsets from the reference or undeformed sample image and subsequent deformed images using the correlation algorithm provides full-field displacements and strains. The stereo-setup of two high-speed cameras from two slightly distinct viewpoints enables to capture the out-of-plane displacement. The stereo-DIC algorithm relates the in-plane and out-of-plane displacement fields denoted as $u(x, y)$, $v(x, y)$ and $w(x, y)$ respectively, by minimizing a similarity criterion between the reference and deformed subsets. The full-field displacement measurements are then used to compute the in-plane Lagrangian strains. 3D calibration plates supplied by LaVision were used to conduct image calibration prior to testing, and a pinhole camera model was used to fit the calibration parameters. The choice of the correlation parameters is critical to obtain consistent mechanical response especially near the centre of impact. The rear surface of the target plate was daubed with a random pattern of white or black dots to aid the image correlation. A subset size of 15 pixels and step parameters (Ns = 4 pixels in x and y directions) were defined as a balance between spatial resolution and precision.

A series of 42 medium velocity impact experiments were conducted on different targets. These include monolithic steel and composite plates as well as the hybrid laminates. Three tests were conducted for each configuration at two different velocities. The experimental matrix with a list of the targets is shown in Table 1. The Steel-Flax (SF) and Flax-Steel (FS) are the same hybrid construction and the difference is the impacted side, i.e. the SF plate is impacted on the steel side and the FS plate is impacted on the flax composite side.

The impacted samples were inspected visually to observe the damage in the samples and additionally an Alicona InfiniteFocus G5 3D profilometer was used to measure the surface profile of the samples.

2.4. Development of finite element model of impact of hybrid laminates

The numerical modelling of FRP composites can be conducted in different scales: micro, meso and macro scale. A macroscopic approach where the composite was modelled with layered shell elements was adopted in this study. The impact response of the monolithic and hybrid composite plates was examined using Finite element simulations in Abaqus Explicit software. The geometry of the target plate and projectile is shown in Fig. 2. The 9 mm diameter projectile is modelled with 1813 R3D4 (4-node bilinear rigid quadrilateral) elements. The projectile was modelled as a mass and an inertia at its centre of mass (m = 2.98 g). The target was

Table 1
Schematic of different target plates for impact testing.

Monolithic	Hybrid
Steel (SS) 	Steel-Flax(SF) 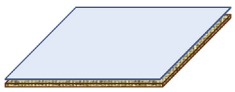
Glass-epoxy composite (GC) 	Flax-Steel (FS) 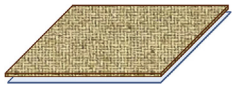
Flax-epoxy composite (FC) 	

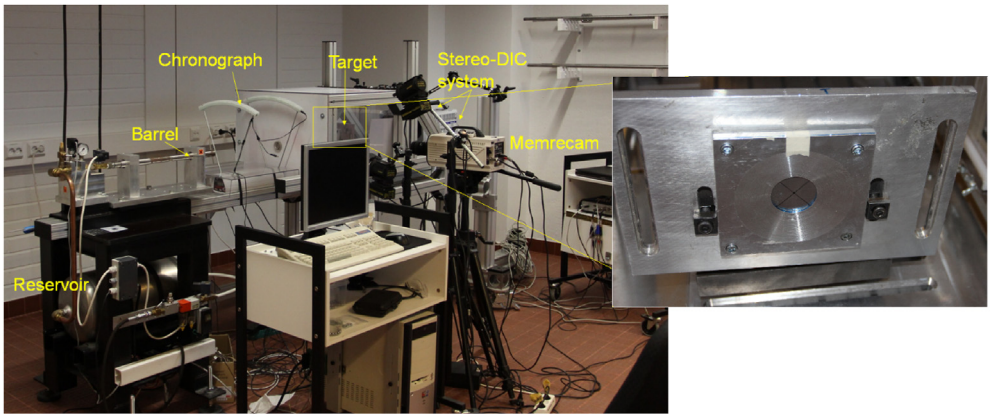

Fig. 1. Experimental setup for impact testing; (inset) fixture for clamping the target plate.

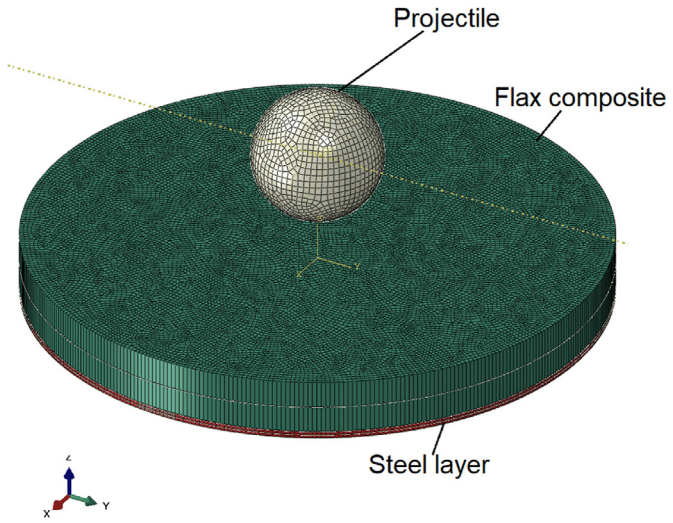

Fig. 2. Geometry and mesh of the finite element model of impact of hybrid laminate.

modelled as circular plates of 40 mm diameter and the support fixture used in the experiment to clamp the target plate was idealised with a clamped boundary condition of the circular edge to reduce the number of elements. Reduced order shell elements (S4R) were used to model both the steel and the composite layers. A mesh sensitivity analysis was performed by increasing the number of elements in the plate from 500 to 10,000 and an optimal mesh size was chosen to provide the best compromise between accuracy of the local material fracture representation and computation time. A fine mesh with average element size of 0.3 mm was defined in the region of the impact, and the resulting model (31,645 quad elements) was used in all subsequent analyses. An initial velocity was defined to the nodes in the spherical projectile. A penalty contact was defined between the target and the projectile. A surface based Cohesive contact model with traction separation law was used to simulate the bonded interface between the steel layer and the composite layer. The cohesive contact uses damage constitutive law for the initiation and evolution of debonding similar to the cohesive element approach. There is literature [31] showing that the surface-based cohesive contact model can predict peak force and displacements reasonably accurately and is easier to be implement. Therefore this approach was adopted for this model.

The progressive damage of the composite material was simulated using in-built constitutive material models in Abaqus. The elastic properties of the composite were defined with orthotropic material parameters, and the onset of damage was defined using a Hashin 2D damage criteria. The Hashin criterion considers different damage initiation mechanisms, namely, fibre tension, fibre compression, matrix tension, matrix compression and shear.

Hashin's damage initiation criteria:

$$F_{fibre\_tension} = \left(\frac{\sigma_{11}}{X_T}\right)^2 + \alpha\left(\frac{\sigma_{12}}{S_L}\right)^2 = 1 \quad (1)$$

$$F_{fibre\_compression} = \left(\frac{\sigma_{11}}{X_C}\right)^2 = 1 \quad (2)$$

$$F_{matrix\_tension} = \left(\frac{\sigma_{22}}{Y_T}\right)^2 + \left(\frac{\sigma_{12}}{S_L}\right)^2 = 1 \quad (3)$$

$$F_{matrix\_compression} = \left(\frac{\sigma_{22}}{Y_C}\right)\left[\left(\frac{Y_C}{2S_T}\right)^2 - 1\right] + \left(\frac{\sigma_{22}}{2S_T}\right)^2 + \left(\frac{\sigma_{12}}{S_L}\right)^2 = 1 \quad (4)$$

where, X_T, Y_T, X_C, Y_C, S_L, and S_T are the strengths in tension, compression and shear in the longitudinal and transverse directions. The damage is initiated when one of the criteria reaches a value of 1 and the softening effect of damage is taken into account by reducing the values of stiffness coefficients using a continuum damage mechanics approach developed by Matzenmiller and widely adopted for composites modelling. A linear softening based on energies dissipated during damage for fibre tension/compression, matrix tension/compression failure modes is used to model the damage evolution. A more detailed description of the Hashin failure criterion in modelling of composites can be found in Ref. [32]. The material parameters for the GFRP and flax-epoxy composite at the ply level were obtained from the literature [33,34] and are shown in Table 2.

In the case of the ferritic stainless steel layer, a rate-sensitive Johnson Cook (JC) constitutive material model was used to define the material behaviour. The JC material model is a phenomenological model that relates the stress in the material to yield stress at a reference temperature (A), strain hardening parameter (B), equivalent plastic strain (ε_p), strain rate constant (C), strain hardening exponent (n), and thermal softening constant (m).

$$\sigma_0 = \left(A + B(\varepsilon_p)^n\right)\left(1 + C\,ln\left(\frac{\dot{\varepsilon_p}}{\dot{\varepsilon}_0}\right)\right)\left(1 - (T)^m\right) \quad (5)$$

The JC material model is widely used to model the elastoplastic behaviour of metals especially at high deformation rates. The parameters used to simulate the stainless steel layer were obtained from Korkmaz [35] and are given in Table 3.

3. Results and discussion

3.1. Results of experimental impact test

Fig. 3 shows typical series of images from the Memrecam showing the impact and rebound of the projectile. The time interval between each image is 0.5 ms (or every 5th frame from the camera capturing at 10,000 fps). The projectile comes into the field of view in frame (a) and is accelerating towards the target. It is possible to track the projectile using imaging software and to follow the position of the projectile in frames (b), (c) and (d) to calculate the initial velocity and therefore the kinetic energy of the projectile just before contact with the target plate. The images (e), (f) and (g) show the rebound of the projectile after the deformation of the plate. The rebound velocity calculated from the position of the projectile was used to estimate the energy dissipated during the impact.

Table 2
Material parameters used for GFRP and flax-epoxy composites.

Property	GFRP composite	Flax-epoxy
E1 (GPa)	44.7	22.3
E2 (GPa)	12.7	4.2
G12(GPa)	5.8	1.97
G23(GPa)	4.5	1.38
σ1t (MPa)	1020	287.7
σ1c (MPa)	620	127.1
σ2t (MPa)	80.9	34
σ2c (MPa)	140	80
σs (MPa)	48.6	37.4

Table 3
Material parameters used for stainless steel [35].

Property	Steel
E (GPa)	200
A (MPa)	359
B (MPa)	327
n	0.454
C	0.0786
m	0.919

Fig. 4 shows typical images of the rear surface of a flax composite target obtained from the high speed cameras. The beginning of the impact where a clear displacement is seen on the rear surface (0.016 ms after contact) was chosen as the first image and the time interval for the subsequent images shown was 0.083 ms (10 frames interval). The progression of the z-displacement through the loading and unloading of the composite is not evident from the raw images. However, the displacement contours obtained from the DIC software for the corresponding images clearly shows the deformation. In image (a) there is initiation of contact between the projectile and the target. The central displacement increases to 3 mm and then 4 mm in the images (b) and (c). The peak displacement of approximately 4.2 mm is reached in image (d) followed by unloading of the composite. The residual displacement in the central localised region of the target after full unloading is visible in image (e). The advantage of using the stereo-DIC system is clear as it enables recording the full-field displacement history of the target.

3.1.1. Impact of monolithic plates

Fig. 5 shows the time history of central displacement of the monolithic steel, GFRP and flax composite targets for a 3 J impact. The out-of-plane displacement in the steel target increases almost linearly till a peak value is reached and followed by an unloading phase. It can be seen that there is some plastic deformation in the target visible as residual displacement. The total duration of the impact is approximately 0.4 ms. The Figure also shows the repeatability of the behaviour for the lower energy impact. The impact response of the GFRP is symmetric, suggesting an elastic impact. Even though the maximum displacement is similar to that of the steel target, the duration of the impact is shorter and the displacement returns to zero at the end of unloading. The displacement history of the flax composite shows similar linear increase up to 0.1 ms but there is some failure initiation at this point which results in oscillations in the curve. The maximum displacements reached for the flax composites are much higher than the peak displacements for the steel target. There is some variation in the post-peak behaviour in the flax composites.

The use of the high speed cameras allow full-field displacement measurement and it is possible to analyse not only the central displacement but the displacement profile of the entire plate to understand the global response. The displacement contour for a typical 3 J impact of flax composite and a waterfall plot showing the progression of the displacement for points along the diameter of the target are shown in Fig. 6. It can be seen that at time t = 0.016 ms, there is a noticeable contact between the projectile and the target, and as time increases, the displacement increases progressively. It is important to note that the deformation is not limited to a small area around the projectile contact but there is global bending in the plate. The waterfall plot only shows the profile during the loading phase up to the peak displacement and the unloading part is not shown. The displacement decreases gradually during the unloading but does not reach zero as there is still some residual displacement due to plastic deformation and damage.

A comparison of the time history of the central displacement and the profile of the z-displacement at maximum displacement for the different monolithic plates are shown in Figs. 7 and 8 for the 3 J and 8 J impact cases respectively. It can be seen that the GFRP plate has the smallest displacement of the monolithic plates with maximum displacements of 2.3 mm and 3.2 mm for the 3 J and 8 J impacts respectively. The steel plate has similar maximum displacement (2.7 mm and 4 mm) but exhibit large plastic deformation at the end of unloading (0.65 mm). For the GFRP plate, the displacement returns to zero on unloading, which indicates good damage tolerance at the tested energy levels. In contrast, the weakness of the flax composite compared to the steel and GFRP is evident with the large displacement and the penetration failure at 8 J impact which is visible as a discontinuity.

The visual inspection of the impacted (front) and rear sides of the monolithic plates after the 8 J impacts are shown in Fig. 9, and it can be seen that the steel target has a local indentation at the point of impact as well as global plastic deformation that is visible as a bulge in the rear surface. The outline of the clamping area is visible as a circle. The GFRP target shows no indentation or visible fibre failure in the outer plies. In contrast, the fibre failure and penetration are evident in both the front and rear surfaces of the flax composite.

3.1.2. Impact of hybrid laminates

The main objective of this paper is to investigate if the hybridisation of the flax composite with a steel layer will result in improvement of the impact resistance. The steel-biocomposite

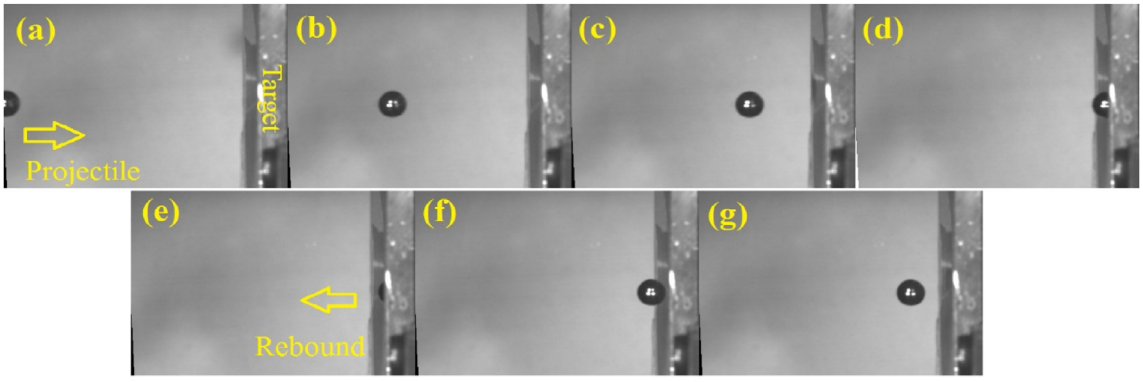

Fig. 3. Typical high speed images from the Memrecam camera showing projectile impact and rebound.

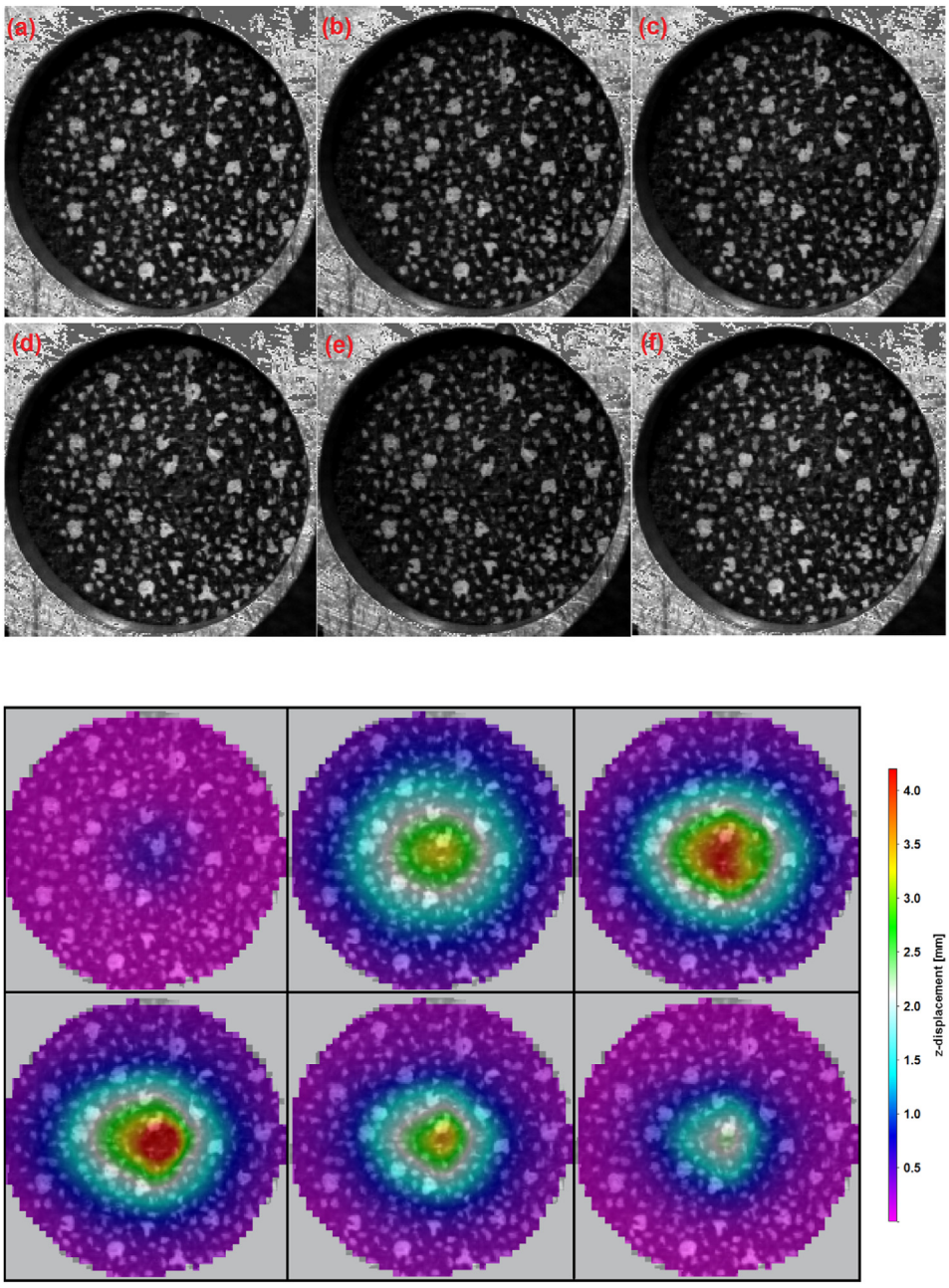

Fig. 4. Typical high speed camera images of the rear surface of the target and the corresponding z-displacement contours obtained from DIC.

hybrid plate was tested in two configurations; namely with the impact on the composite side and the impact on the steel side. Fig. 10 shows a comparison of the central displacement history for the two hybrid configurations with monolithic flax composite and GFRP target. It can be seen that the addition of the steel layer dramatically improves the impact resistance compared to the monolithic flax composite. The maximum displacements of the flax composite of 4.95 mm and 9.57 mm were reduced to 1.45 mm and 2.2 mm for flax-steel hybrid plates for the 3 J and 8 J impact, respectively. The lower displacement is a good indicator of reduced damage in the hybrid laminate. This improvement is also critical that the deformation of the hybrid plates is even lower than the GFRP composite. This proves that biocomposite hybrids can potentially be used to replace traditional synthetic fibre composites in structural applications.

It can also be noted from the comparison of the hybrid configurations in Fig. 10, that there is no significant effect of the configuration as evidenced by the similar displacement history of the flax - steel and steel - flax hybrid for both energies. A visual inspection of the hybrid plates after 8 J impact shows that there is no significant damage in the flax composite for both cases (Fig. 11). The hybrid composite with the impact on the flax side shows a discolouration in the centre of the plate at the point of impact suggesting local matrix damage. It is not possible to observe visually any damage on the rear side of the hybrid plate on the steel side. Similarly, there is localised indentation in the steel layer on the steel – flax hybrid composite and no observable damage on the rear flax composite side.

Fig. 12 shows the profilometer contours of the flax composite and the hybrid composites for 8 J impact. The penetration failure of

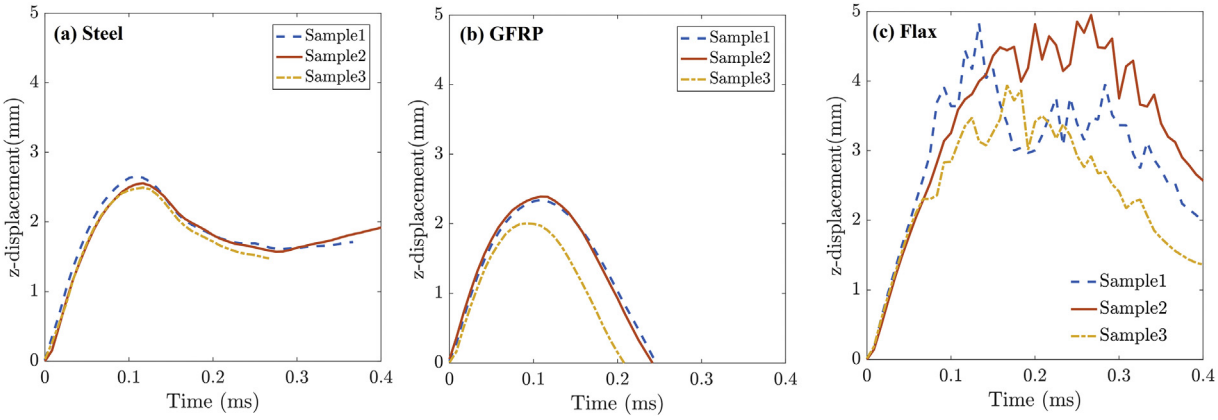

Fig. 5. Displacement history for 3 J impact for (a) steel, (b) GFRP and (c) flax composite target.

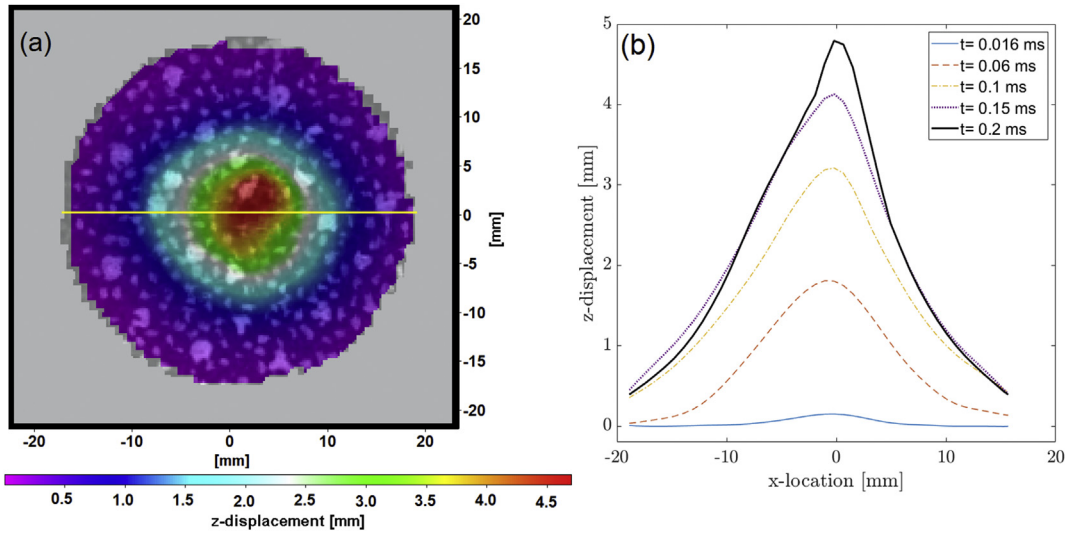

Fig. 6. Displacement contour and waterfall plot along the yellow line in Figure (a) for a 3J impact of flax composite.

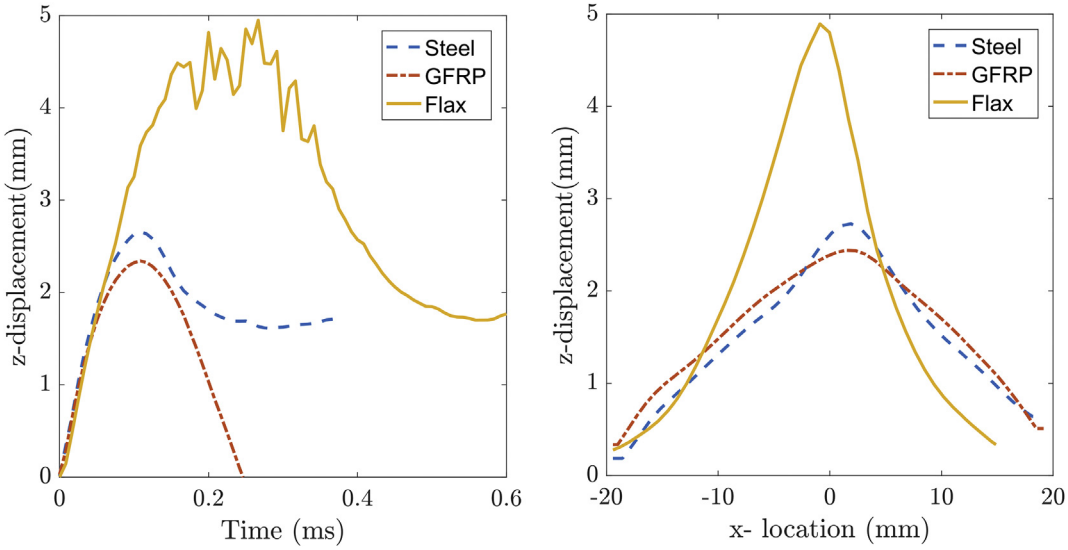

Fig. 7. Comparison of displacement history and profile for 3 J impact.

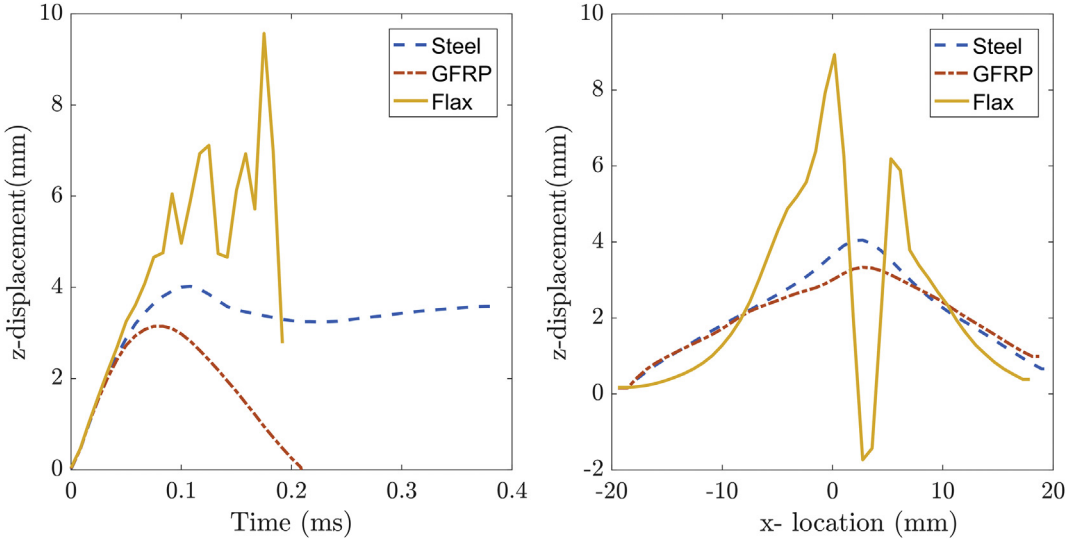

Fig. 8. Comparison of displacement history and profile for 8 J impact.

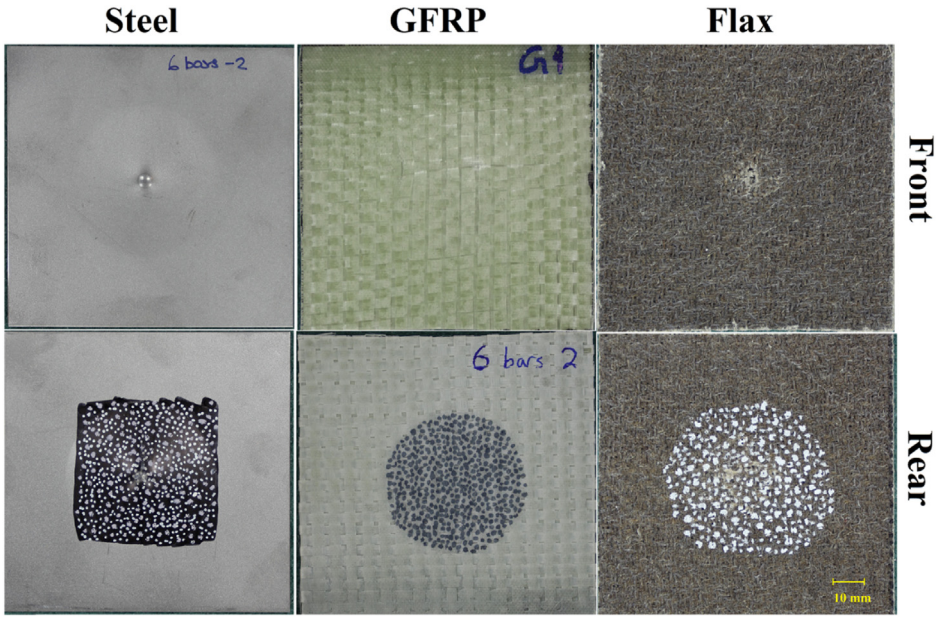

Fig. 9. Photographs of samples after 8 J impact.

the flax composite is clearly visible and the peak residual displacement in the monolithic flax target is more than 3.5 mm. The residual displacements in the flax – steel and steel – flax hybrid composites were 2 and 2.2 mm, and based on the surface profile it can be proposed that it is marginally better to have the composite target on the impacted side. The metal layer is more ductile and is better suited to be on the rear surface which has larger tensile stresses during the plate bending. However, this needs to be verified with impacts at higher energies and with numerical modelling.

The impacted samples were cut close to the impact zone and embedded in a clear epoxy resin for cross-sectional analysis to observe the damage mechanisms in the flax composite and hybrid samples. The embedded samples were ground and polished for optical microscopy. The cross-section views of the targets are shown in Fig. 13. The fibre failure and perforation in the monolithic flax composite can be observed in the micrographs. In the case of the flax-steel hybrid (i.e. impacted on the composite side), there is a sizeable area of debonding between the composite and metal layers. This debonding typically occurs during the unloading phase of the impact where the composite layer recovers from the peak displacement. There is no corresponding debonding zone observed in the hybrid composite with the steel layer in the impacted side but there is a more local indentation zone in the steel layer which is constrained by the composite backing. It is clear that the hybrid composites have different mechanisms for damage and energy absorption depending on which layer is impacted first.

3.1.3. Dissipated energy

The initial and rebound velocities measured from the Memrecam images were used to calculate the initial kinetic energy and rebound energy. For instance, the initial velocity for a flax

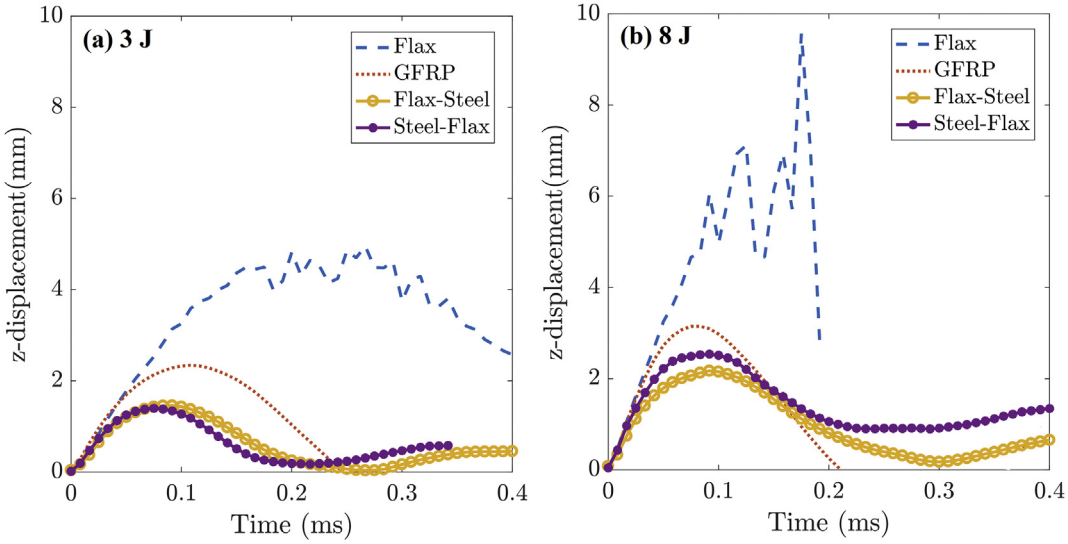

Fig. 10. Comparison of the displacement histories of hybrid composites for 3 J and 8 J impacts.

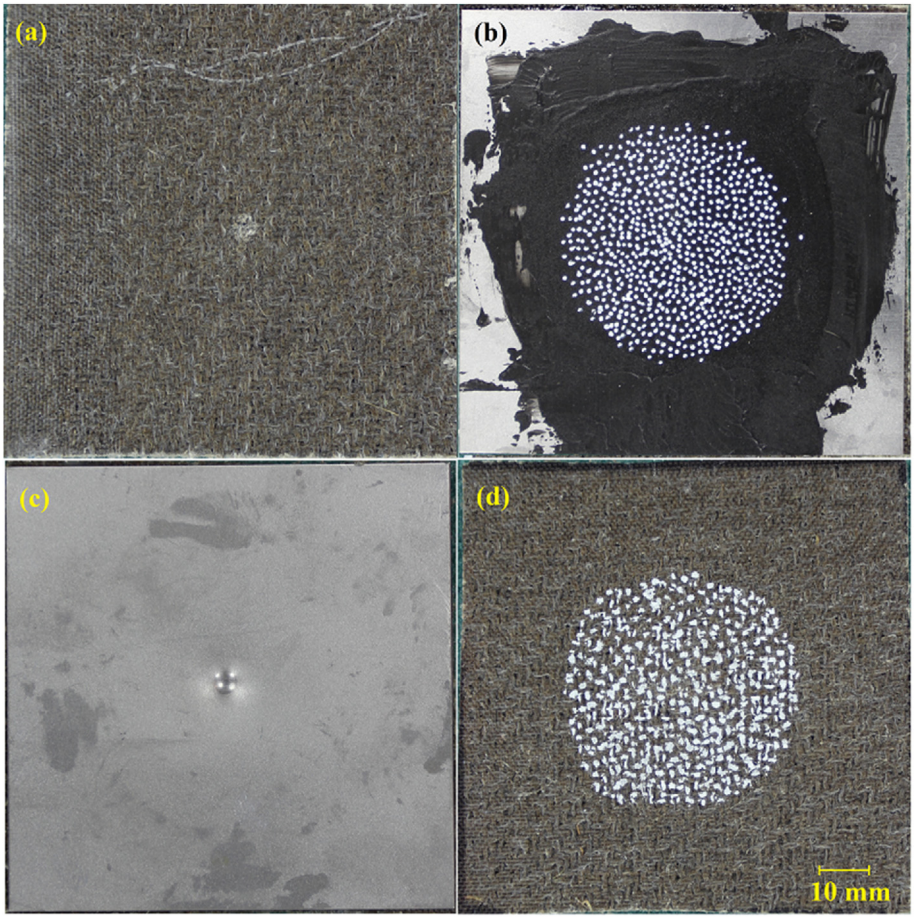

Fig. 11. Photographs of hybrid targets after 8 J impact (a,b) flax - steel hybrid and (c,d) steel-flax hybrid.

composite target impacted by accelerating the projectile with 0.2 MPa pressure was 45.72 m/s. Since the mass of the projectile is 2.98 g, the initial kinetic energy was calculated as 3.12 J. In this case the projectile rebounded after impact with a velocity of 14.3 m/s. This meant that the residual energy of the projectile was 0.31 J. The dissipated energy is the difference between the kinetic and rebound energy. A perfectly elastic impact would mean that the rebound velocity was the same as the initial velocity and there would be no energy lost. However, in real impact, some of the energy is absorbed by the target through plastic deformation and

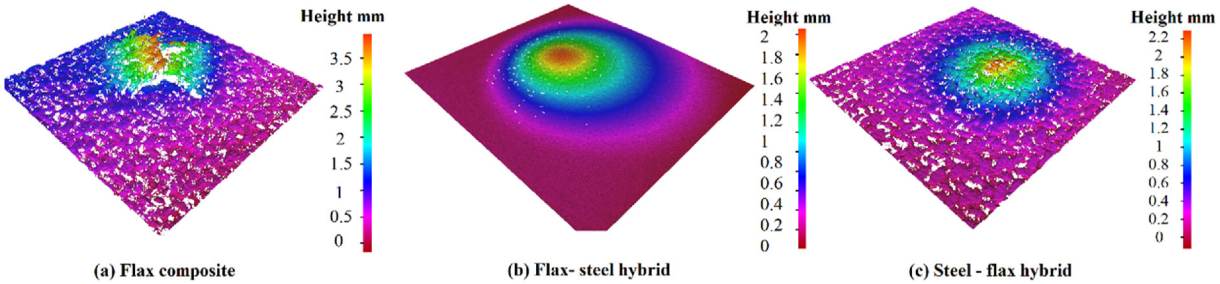

Fig. 12. Surface profiles of the impacted samples obtained from Alicona Profilometer.

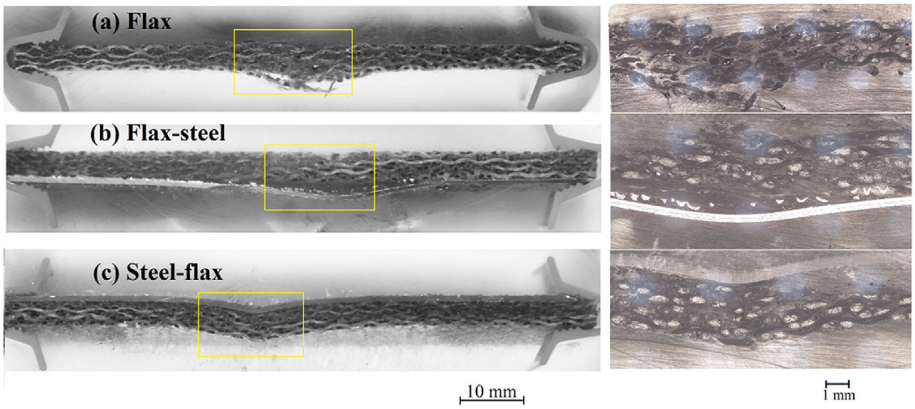

Fig. 13. Cross-section views of the samples after 8 J impact (a) flax composite, (b) flax-steel and (c) steel-flax.

damage and some energy is dissipated in friction and heat. Fig. 14 shows the dissipated energy as a percentage of the initial kinetic energy. It can be seen that nearly 90% of the initial kinetic energy is dissipated in the case of a steel target impacted at 3 J and this increases to 95% for 8 J impact. The ductile nature of the metals means that large amount of energy is absorbed through bending and plastic deformation. The GFRP target dissipates the least amount of energy with 66% and 80% for the 3 J and 8 J impact. This is supported by the minimum damage observed in the GFRP targets. The energy dissipated in the 8J impact of flax composite is said to have reached 100% as there is complete penetration of the composite and no rebound of the projectile. In reality, there is a residual velocity in the projectile after penetration of the target but the camera setup does not support measuring the residual velocity. The main outcome of the energy analysis is that the hybrid configurations of flax-steel and steel-flax avoids the penetration failure and there is reduction in the dissipated energy implying less damage to the composite. The dissipated energy is comparable to monolithic steel even though it is still higher than that of GFRP target.

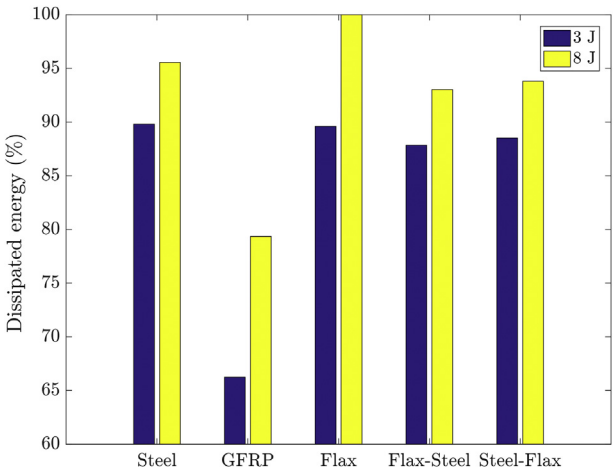

Fig. 14. Comparison of dissipated energy for different targets.

3.2. Results of the finite element model

Typical results from the Finite element simulation of the impact of a steel target are shown in Fig. 15. The progression of the out-of-plane displacement (z-disp) contours show the impact loading and unloading of the target due to the rebound of the projectile. The time corresponds to different instances from the beginning of contact to the end of contact (dt = 0.05 ms). The localised deformation in the steel target at the point of contact and the global bending of the plate can be observed. It can also be seen that there is a large residual displacement in the steel target due to plastic deformation.

The total duration of the impact simulation was 0.3 ms. Fig. 16 summarises the results of the central displacement obtained from the FE simulation of monolithic plates for 3 J and 8 J impact. It can be seen that the steel target shows plastic deformation in the target visible as residual displacement similar to the experimental data. The shorter impact duration and nearly symmetric impact response of GFRP observed in the experiments is also captured in the FE model. The displacement history of the flax composite shows similar linear increase but the failure initiation and resulting oscillations in the curve observed in the experiment are not reproduced in the simulation.

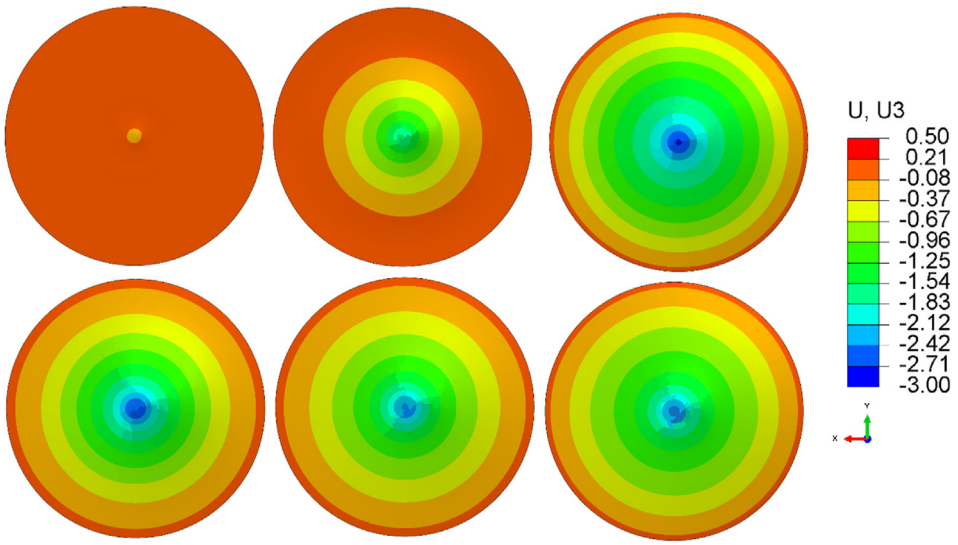

Fig. 15. Displacement contours obtained from FE simulation of steel target for 3 J impact (dt = 0.05 ms).

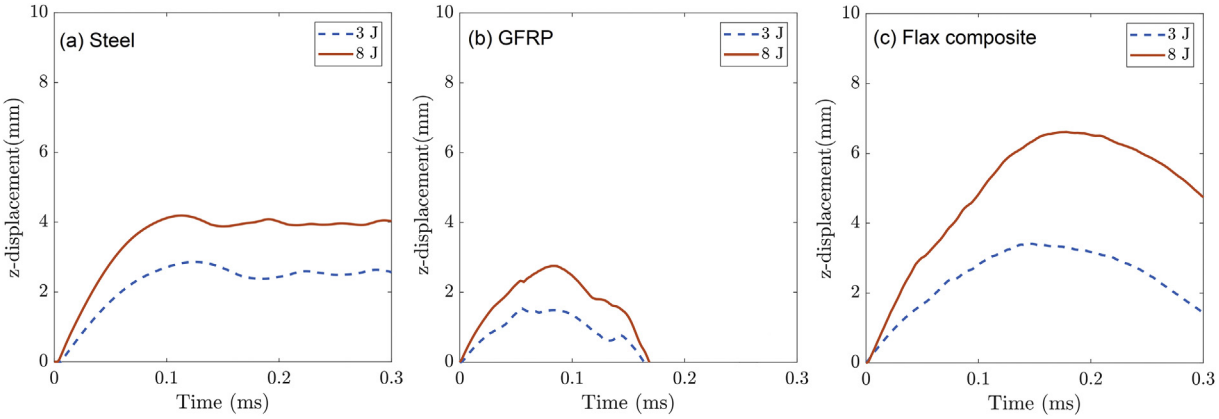

Fig. 16. Displacement history of (a) steel, (b) GFRP and (c) flax composite target from FE simulation.

3.2.1. Validation of FE model for monolithic targets

The validation of the FE model is conducted by comparing the displacement histories with the experimental data obtained from the DIC. A detailed comparison of the displacement history results from the simulation and from the experiment is shown in Fig. 17. The dashed lines correspond to experimental data and the solid lines are for the simulation results. The predicted displacements for the flax composites are underestimated for both the 3 J and 8 J impact compared to the peak observed in the experiments.

The damage modes of the flax composite after 8 J impact is shown in Fig. 18. It corresponds to the fibre compressive, fibre tensile, matrix compressive and matrix tensile modes, respectively. It can be seen that there is extensive damage in the composite. The rear face damage in the flax composite is predominantly fibre-controlled due to the lower strength of flax fibre. This results in fibre breakage with no apparent delamination as evident from the fibre tensile damage shown in Fig. 19 (b). This shows that the layered shell approach is still capable of capturing the main failure events occurring in the composite plate during impact.

3.2.2. Validation of FE model for hybrid targets

A comparison of the displacement history obtained from the simulations of the Flax-Steel and Steel-Flax hybrid composites with experimental DIC results was also conducted for the validation of the finite element model of the impact of hybrid composites. The displacement history from the simulations are shown in solid lines and the experimental results in dashed lines in Fig. 19. The results from the Abaqus model has generally good agreement with the experimental data. The maximum displacement obtained from the model show good agreement for the 3 J impact case for both the flax-steel and steel-flax configurations. The unloading phase is not fully represented as the displacement from the steel rear surface has large plastic deformation. There is reasonable agreement for the 8 J impact case, with the steel-flax hybrid having better agreement than the flax-steel. It should be noted that the macroscopic modelling approach adopted in this study with a layered shell model has certain limitations in its capability to describe the through-thickness behaviour of the composite. Also, the delamination failure in the composite cannot be adequately simulated with the layered shell. Dlugosch et al. [20] found similar agreement between simulation using two layered shell elements with a simplified interface model and experiment of crashworthiness of hybrid FRP-steel sections and reported that considering the complexity of the physical damage mechanisms and the interaction between the material phases, the simplified modelling approach was applicable for evaluation of structural concepts.

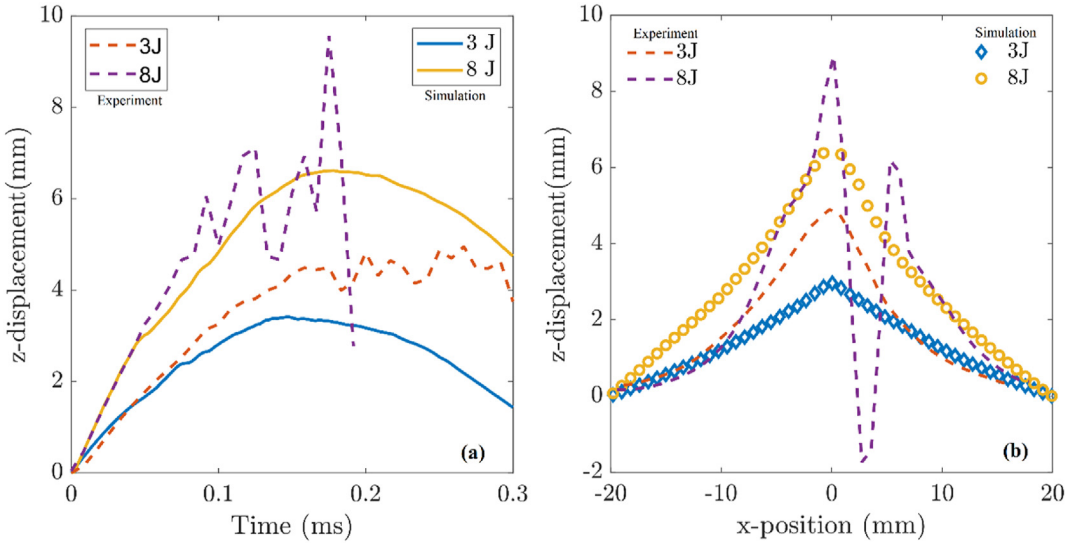

Fig. 17. Comparison of (a) displacement history and (b) displacement profile of flax composite after 3 J and 8 J impact.

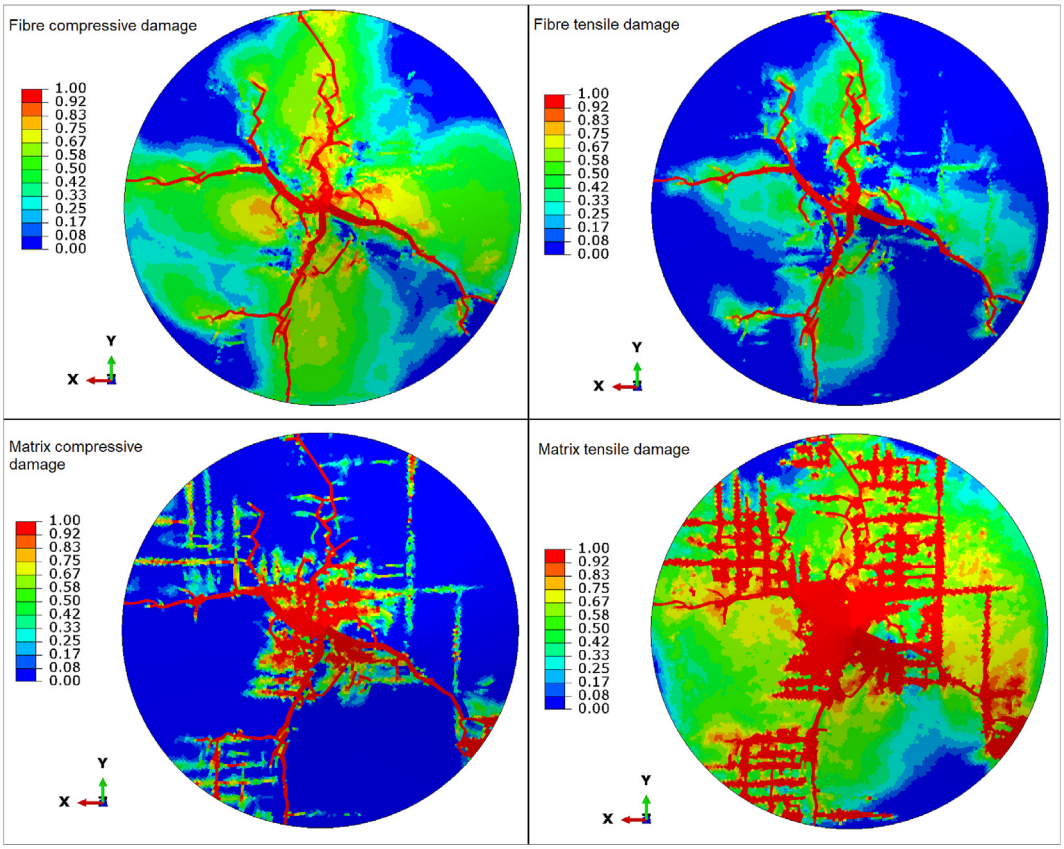

Fig. 18. Failure contours of flax composite after 8 J impact.

3.3. Parametric study of impact behaviour of hybrid laminates

The validated FE model was then used to study the evolution of deflection of the hybrid laminate for different energies of impact. Fig. 20 (a) shows the z-displacement of the Flax-Steel hybrid for initial velocities from 45 m/s to 120 m/s, which correspond to impact energies ranging from 3 J, to 21.5 J. It is clear that the maximum displacement and residual displacement increase with increasing energy of impact. The difference in the behaviour of the hybrid laminate impacted on the flax side and steel side are evident from Fig. 20 (b). It can be seen that at lower energy of 3 J, there is no substantial difference between the Flax-Steel and Steel-Flax but at higher energies, the hybrid configuration with impact on the composite has lower deflection compared to the impact on the steel side.

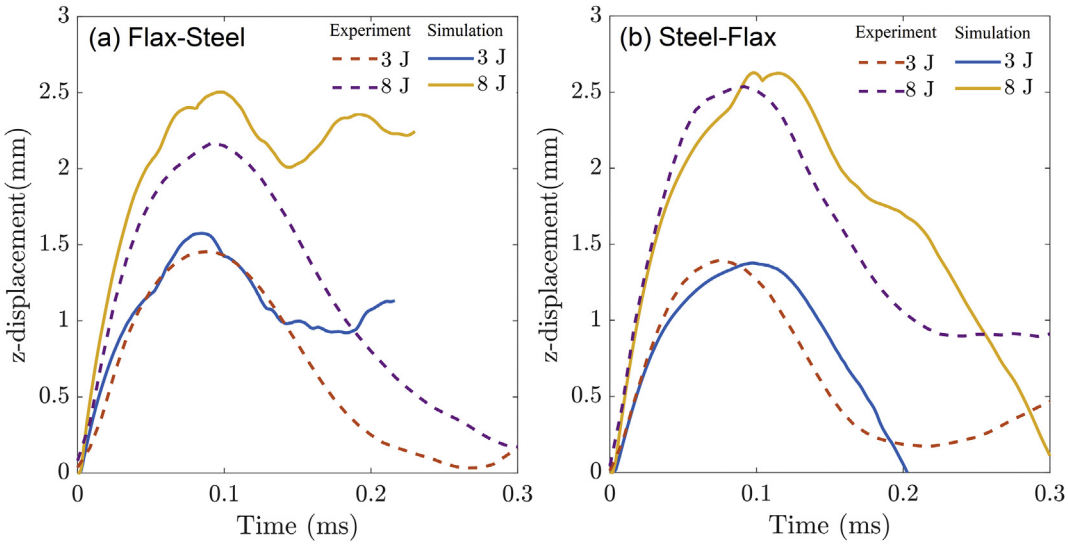

Fig. 19. Comparison of displacement histories for (a) flax-steel and (b) steel-flax hybrid composites.

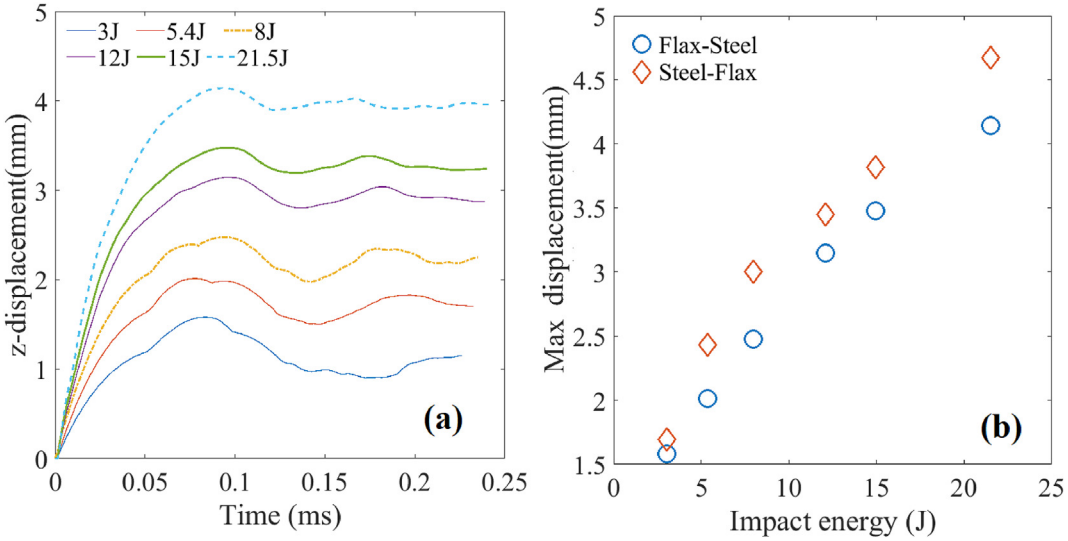

Fig. 20. (a) Evolution of displacement for different impact energies for flax-steel hybrid and (b) comparison of maximum displacement for flax-steel and steel-flax hybrid composites.

The effect of the thickness of the steel layer on the impact response of the Flax-Steel hybrid composite was also explored with the FE model. The displacement history of the hybrid composite with different thickness of steel layer (0.2 mm, 0.3 mm, 0.5 mm and 0.6 mm) was compared to the displacement history of monolithic flax composite plate (Fig. 21). It can be seen that the addition of even a thin layer of 0.2 mm of steel substantially reduces the deflection in the plate. The increased thickness of the steel layer further reduces the deflection in the hybrid laminate. This is in agreement with the results of Yiben et al. [21], who found the steel thickness in FRP-steel hybrid had a significant effect on the damage area. The lower deflection and damage area of the hybrid laminate will result in higher residual strength [19]. These results confirm the hypothesis that the addition of a steel layer to the natural fibre composite to create a hybrid laminate is a successful strategy to improve the impact damage resistance of biocomposites. The validated FE model can also be used to find optimal configurations of the hybrid composite for weight and strength requirements of particular applications.

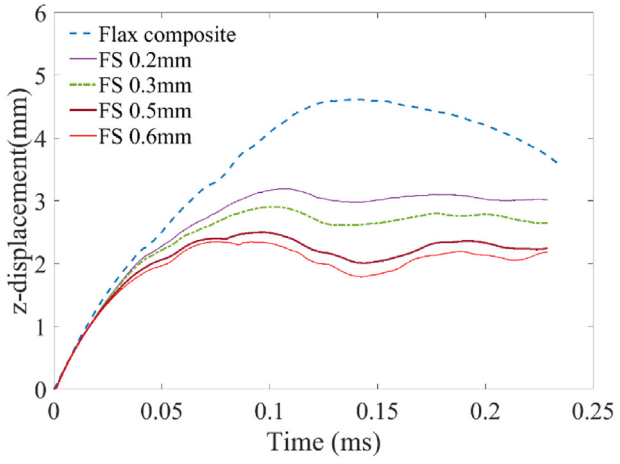

Fig. 21. Comparison of displacement history for different thickness of steel layer.

There are still some potential improvements to the accuracy of the model planned for future work. In particular, the present model does not explicitly model the adhesive layer between the composite and the steel layers. During et al. [19] reported that the plastic deformation of the steel layers and the presence of high shear stresses at the steel-composite interface results in delaminations and subsequently higher absorbed energy. The inclusion of debonding failure between the steel and biocomposite will improve the accuracy of the predictive model.

4. Conclusions

The objective of this article was to explore the improvement in impact resistance of natural fibre composites by hybridisation with metal layer. An experimental campaign of medium velocity impact testing was used to compare hybrid laminates made of adhesively bonded flax-epoxy composite and stainless steel layers to traditional glass fibre composites. The experimental setup consisted of a high velocity particle impactor and a high speed imaging system including two Photron cameras monitoring the rear surface of the impacted target and a Memrecam camera to measure the initial and rebound velocities. Finite element modelling of the composite and hybrid targets was accomplished using Abaqus Explicit software. The results of the impact experiments show that the monolithic biocomposite exhibits fibre failure and perforation even at low energy of impacts while the failure mode of matrix cracking and delamination was observed in GFRP plates. The key outcome of the research was that the hybrid configuration with the steel layer significantly reduced the deformation and damage in the flax-composite compared to monolithic plates. Another outcome was the investigation of the effect of the impact configuration with steel or composite layer on the impacted side. Even though the maximum displacement was similar for the two configurations, the configuration with the flax composite layer on the impact side was shown to lead to different failure modes compared to the construction with steel front layer. The composite in front of the metal layer spreads the impact load over a wider area and is an efficient approach to improve the impact resistance of the hybrid plate. The FE model is validated by comparing the displacement histories and failure modes and the model is used to study the effect of impact energies and thickness of steel layer. This paper demonstrates the potential of hybridisation with metal layer in improving the impact resistance of biocomposites, and is an important contribution to the widespread adoption of biocomposites in structural applications.

Conflict of interest

The authors declare that there is no conflicts of interest.

Acknowledgments

KRR would like to acknowledge the Marie Curie Individual Fellowship funded by the European Union's H2020-MSCA-IF-2018 Programme (FIDELITY project, grant agreement n◦ 846458).

References

[1] D.U. Shah, P.J. Schubel, M.J. Clifford, Can flax replace E-glass in structural composites? A small wind turbine blade case study, Compos. B Eng. 52 (2013) 172–181, https://doi.org/10.1016/j.compositesb.2013.04.027.
[2] L. Yan, N. Chouw, K. Jayaraman, Flax fibre and its composites - a review, Compos. B Eng. 56 (2014) 296–317, https://doi.org/10.1016/j.compositesb.2013.08.014.
[3] L. Pil, F. Bensadoun, J. Pariset, I. Verpoest, Why are designers fascinated by flax and hemp fibre composites? Composer Part A Appl Sci Manuf 83 (2016) 193–205, https://doi.org/10.1016/j.compositesa.2015.11.004.
[4] A. Bourmaud, J. Beaugrand, D.U. Shah, V. Placet, C. Baley, Towards the design of high-performance plant fibre composites, Prog. Mater. Sci. 97 (2018) 347–408, https://doi.org/10.1016/j.pmatsci.2018.05.005.
[5] K.R. Ramakrishnan, S. Corn, N. Le Moigne, P. Ienny, P. Slangen, Experimental assessment of low velocity impact damage in flax fabrics reinforced biocomposites by coupled high-speed imaging and DIC analysis, Composer Part A Appl Sci Manuf 140 (2021), https://doi.org/10.1016/j.compositesa.2020.106137.
[6] C. Santulli, Falling weight impact damage characterisation on flax/epoxy laminates, Int. J. Mater. Prod. Technol. 36 (2009) 221–228.
[7] G. Park, H. Park, Structural design and test of automobile bonnet with natural flax composite through impact damage analysis, Compos. Struct. 184 (2018) 800–806, https://doi.org/10.1016/j.compstruct.2017.10.068.
[8] S. Liang, L. Guillaumat, P.B. Gning, Impact behaviour of flax/epoxy composite plates, Int. J. Impact Eng. 80 (2015) 56–64, https://doi.org/10.1016/j.ijimpeng.2015.01.006.
[9] F. Bensadoun, D. Depuydt, J. Baets, I. Verpoest, A.W. van Vuure, Low velocity impact properties of flax composites, Compos. Struct. 176 (2017) 933–944, https://doi.org/10.1016/j.compstruct.2017.05.005.
[10] A.K. Barouni, H.N. Dhakal, Damage investigation and assessment due to low-velocity impact on flax/glass hybrid composite plates, Compos. Struct. 226 (2019) 111224, https://doi.org/10.1016/j.compstruct.2019.111224.
[11] B.L. Sy, Z. Fawaz, H. Bougherara, Damage evolution in unidirectional and cross-ply flax/epoxy laminates subjected to low velocity impact loading, Composer Part A Appl Sci Manuf 112 (2018) 452–467, https://doi.org/10.1016/j.compositesa.2018.06.032.
[12] M. Ravandi, W.S. Teo, L.Q.N. Tran, M.S. Yong, T.E. Tay, Low velocity impact performance of stitched flax/epoxy composite laminates, Compos. B Eng. 117 (2017) 89–100, https://doi.org/10.1016/j.compositesb.2017.02.003.
[13] H.K. Patel, G. Ren, P.J. Hogg, T. Peijs, Hemp fibre as alternative to glass fibre in sheet moulding compound Part 1 – influence of fibre content and surface treatment on mechanical properties, Plast Rubber Compos 39 (2010) 268–276, https://doi.org/10.1179/174328910X12647080902853.
[14] E. Selver, H. Dalfi, Z. Yousaf, Investigation of the impact and post-impact behaviour of glass and glass/natural fibre hybrid composites made with various stacking sequences: experimental and theoretical analysis, J. Ind. Textil. (2020), https://doi.org/10.1177/1528083719900670.
[15] G. Reyes, W.J. Cantwell, The mechanical properties of fibre-metal laminates based on glass fibre reinforced polypropylene, Compos. Sci. Technol. 60 (2000) 1085–1094, https://doi.org/10.1016/S0266-3538(00)00002-6.
[16] T. Pärnänen, M. Kanerva, E. Sarlin, O. Saarela, Debonding and impact damage in stainless steel fibre metal laminates prior to metal fracture, Compos. Struct. 119 (2015) 777–786, https://doi.org/10.1016/j.compstruct.2014.09.056.
[17] E. Sarlin, M. Lindroos, M. Apostol, V.T. Kuokkala, J. Vuorinen, T. Lepistö, et al., The effect of test parameters on the impact resistance of a stainless steel/rubber/composite hybrid structure, Compos. Struct. 113 (2014) 469–475, https://doi.org/10.1016/j.compstruct.2014.03.049.
[18] E. Sarlin, M. Apostol, M. Lindroos, V.T. Kuokkala, J. Vuorinen, T. Lepistö, et al., Impact properties of novel corrosion resistant hybrid structures, Compos. Struct. 108 (2014) 886–893, https://doi.org/10.1016/j.compstruct.2013.10.023.
[19] D. Düring, E. Petersen, D. Stefaniak, C. Hühne, Damage resistance and low-velocity impact behaviour of hybrid composite laminates with multiple thin steel and elastomer layers, Compos. Struct. 238 (2020) 111851, https://doi.org/10.1016/j.compstruct.2019.111851.
[20] M. Dlugosch, J. Fritsch, D. Lukaszewicz, S. Hiermaier, Experimental investigation and evaluation of numerical modeling approaches for hybrid-FRP-steel sections under impact loading for the application in automotive crash-structures, Compos. Struct. 174 (2017) 338–347, https://doi.org/10.1016/j.compstruct.2017.04.077.
[21] Y. Zhang, L. Sun, L. Li, T. Wang, L. Shen, Experimental and numerical investigations on low-velocity impact response of high strength steel/composite hybrid plate, Int. J. Impact Eng. 123 (2019) 1–13, https://doi.org/10.1016/j.ijimpeng.2018.08.015.
[22] M. Vasumathi, V. Murali, Effect of alternate metals for use in natural fibre reinforced fibre metal laminates under bending, impact and axial loadings, Procedia Eng 64 (2013) 562–570, https://doi.org/10.1016/j.proeng.2013.09.131.
[23] H.T.N. Kuan, W.J. Cantwell, M.a. Hazizan, C. Santulli, The fracture properties of environmental-friendly fiber metal laminates, J. Reinforc. Plast. Compos. 30 (2011) 499–508, https://doi.org/10.1177/0731684411398536.
[24] M.R. Abdullah, C.L. Pang, N.A. Husain, B. Abdi, Indentation fracture behaviour of fibre metal laminates based on kenaf/epoxy, Int Rev Mech Eng 8 (2014) 265–270.
[25] P. Wambua, B. Vangrimde, S. Lomov, I. Verpoest, The response of natural fibre composites to ballistic impact by fragment simulating projectiles, Compos. Struct. 77 (2007) 232–240, https://doi.org/10.1016/j.compstruct.2005.07.006.
[26] E. Kandare, S. Yoo, V.S. Chevali, A.A. Khatibi, On the notch sensitivity of flax fibre metal laminates under static and fatigue loading, Fatig. Fract. Eng. Mater. Struct. 41 (2018) 1691–1705, https://doi.org/10.1111/ffe.12807.
[27] C. Santulli, H.T. Kuan, F. Sarasini, I. De Rosa, W. Cantwell, Damage characterisation on PP-hemp/aluminium fibre–metal laminates using acoustic emission, J. Compos. Mater. 47 (2013) 2265–2274, https://doi.org/10.1177/0021998312457098.
[28] K.R. Ramakrishnan, E. Sarlin, M. Kanerva, M. Hokka, Experimental study of adhesively bonded natural fibre composite – steel hybrid laminates,

Composer Part C Open Access 5 (2021) 100157, https://doi.org/10.1016/j.jcomc.2021.100157.
[29] K.R. Ramakrishnan, M. Hokka, E. Sarlin, M. Kanerva, R. Kouhia, V.T. Kuokkala, Experimental investigation of the impact response of novel steel-biocomposite hybrid materials, EPJ Web Conf. 183 (2018) 1–6, https://doi.org/10.1051/epjconf/201818302040.
[30] E. Sarlin, E. Heinonen, J. Vuorinen, M. Vippola, T. Lepistö, Adhesion properties of novel corrosion resistant hybrid structures, Int. J. Adhesion Adhes. 49 (2014) 51–57.
[31] M.Z. Sadeghi, A. Gabener, J. Zimmermann, K. Saravana, J. Weiland, U. Reisgen, et al., Failure load prediction of adhesively bonded single lap joints by using various FEM techniques, Int. J. Adhesion Adhes. 97 (2020) 102493, https://doi.org/10.1016/j.ijadhadh.2019.102493.
[32] R. Bogenfeld, J. Kreikemeier, T. Wille, Review and benchmark study on the analysis of low-velocity impact on composite laminates, Eng. Fail. Anal. 86 (2018) 72–99, https://doi.org/10.1016/j.engfailanal.2017.12.019.
[33] E.J. Barbero, F.A. Cosso, R. Roman, T.L. Weadon, Determination of material parameters for Abaqus progressive damage analysis of E-glass epoxy laminates, Compos. B Eng. 46 (2013) 211–220, https://doi.org/10.1016/j.compositesb.2012.09.069.
[34] Z.E. Cherif, C. Poilâne, A. Vivet, B. Ben Doudou, J. Chen, About optimal architecture of plant fibre textile composite for mechanical and sorption properties, Compos. Struct. 140 (2016) 240–251, https://doi.org/10.1016/j.compstruct.2015.12.030.
[35] M.E. Korkmaz, Verification of Johnson-Cook parameters of ferritic stainless steel by drilling process: experimental and finite element simulations, J Mater Res Technol (2020) 2–10, https://doi.org/10.1016/j.jmrt.2020.03.045.